
FORECASTING THE DYNAMICS OF SEGREGATED POPULATION DISTRIBUTIONS AT THE NEIGHBORHOOD SCALE USING DENSITY-FUNCTIONAL FLUCTUATION THEORY

A PREPRINT

Yuchao Chen^{1,5}, Yunus A. Kinkhabwala^{2,5}, Boris Barron¹, Matthew Hall^{3,4}, Tomas A. Arias¹, and Itai Cohen¹

¹Department of Physics, Cornell University, Ithaca, NY 14853, USA.

²Department of Applied and Engineering Physics, Cornell University, Ithaca, NY, 14853, USA.

³Policy Analysis and Management, Cornell University, Ithaca, NY, 14853, USA.

⁴Cornell Institute for Public Affairs, Cornell University, Ithaca, NY, 14853, USA.

⁵These authors contributed equally to this work.

August 25, 2020

ABSTRACT

Decisions regarding housing, transportation, and resource allocation would all benefit from accurate neighborhood-scale population forecasts. While various forecast methods exist at regional scales, developing a neighborhood-scale forecast remains a challenge, because complex drivers of residential choice ranging from housing policies to social preferences and economic status cumulatively cause drastic neighborhood-scale segregation. Here, we show how to forecast the dynamics of neighborhood-scale demographics by extending a novel statistical physics approach called Density-Functional Fluctuation Theory (DFFT) to multi-component time-dependent systems. In particular, this technique observes the fluctuations in neighborhood-scale demographics to extract effective drivers of segregation. As a demonstration, we simulate a segregated city using a Schelling-type segregation model, and found that DFFT accurately predicts how a city-scale demographic change trickles down to block scales. Should these results extend to actual human populations, DFFT could capitalize on the recent advances in demographic data collection and regional-scale forecasts to generate accurate neighborhood-scale forecasts.

Keywords Statistical physics · Racial residential segregation · Migration · Density-Functional Fluctuation Theory

1 Introduction

Forecasting the neighborhood-scale dynamics of residential populations remains an outstanding problem in demography with the potential to inform and significantly affect local planning of social and economic developments [1]. For example, such forecasts could be used to achieve optimal allocation of educational, health and safety resources by determining the need for new schools [2], hospitals [3] and fire stations [4] in each neighborhood. In addition, such forecasts would be important for estimating housing demands [5], and might help combat racial inequalities by predicting the need for low-income housing developments [6] and public transportation [7, 8]. Despite this wide range of important potential applications, methods for accurate neighborhood-scale population forecasts remain limited.

Importantly, at regional scales, there are already numerous methods for predicting population change and dynamics. Traditionally, the demographic equation is applied to different cohorts [9, 10, 11, 12, 13, 14]. In particular, estimates of birth and death rates from past data are already quite accurate. Models with different amounts of sophistication have

Table 1: List of Important Variables Used

Variable	Meaning	Usage
U_R^{so}	Social Utility for a red agent	
U_B^{so}	Social Utility for a blue agent	
U_R^{sp}	Spatial Utility for a red agent	Schelling
U_B^{sp}	Spatial Utility for a blue agent	
x	Position in Schelling city	
N_R^{ne}	Number of red agents in the 8-connected neighborhood	
N_B^{ne}	Number of blue agents in the 8-connected neighborhood	
b	Block index	
t	Time	
s	Number of empty cells (spaces) in a block	
s_{tot}	Total number of empty cells (spaces) in a city	
N_{tot}	Total number of agents in a city	Schelling
P_b	Probability Distribution of agents in block b	& DFFT
$N_{R,b}$	Number (Density) of red agents in block b	
N_R	Abbreviated $N_{R,b}$ when there is no ambiguity	
$N_{B,b}$	Number (Density) of blue agents in block b	
N_B	Abbreviated $N_{B,b}$ when there is no ambiguity	
z_b	Normalization constant for P_b	
$v_{R,b}$	Vexation for red agents in block b	
$v_{B,b}$	Vexation for blue agents in block b	
f	Frustration	
H_b	Headache function for block b	DFFT
$P_{b \rightarrow b'}$	Probability of transition of an agent from block b to b'	
$\nu_{R,b \rightarrow b'}$	Number (Density) flow rate for red agent from block b to b'	
$\nu_{B,b \rightarrow b'}$	Number (Density) flow rate for blue agent from block b to b'	
μ_R	Red agent potential in a city	
μ_B	Blue agent potential in a city	

also been developed to estimate the migration rates from available data [15]. For example, the gravity model [16, 17, 18, 19, 20, 21] and the gravity-like Weidlich-Haag Migratory Model [22, 23, 24, 25] fit migration data by including relative preferences of origin and destination regions as well as preferences to make moves to closer locations. The challenge then, is how to relate the data at the regional level to forecasts at the neighborhood scale.

One of the key hurdles for making such relations is that at the neighborhood scale drivers of segregation can significantly affect the resulting distributions. At regional scales, most methods either ignore the drivers of segregation [16] or assume some simple forms for such segregation effects [25]. These simplifications are most likely justified for regional or national population forecasts, because the drivers of segregation, such as economic status, social preferences and housing policy [26, 27], usually average over on a large scale. Such simplifications, however, would lead to bigger errors if we apply them to make neighborhood-scale forecasts. For example, consider the recent growth of the Hispanic population in the United States. With traditional methods, demographers were able to predict this growth on the coarser county level, where drivers of segregation are roughly averaged over and can thus be reasonably ignored. On the neighborhood level, however, Hispanic-majority blocks experienced proportionally different growth than Hispanic-minority blocks, suggesting that segregation greatly affects the population dynamics at the block scale. Thus, there is still a need for methods that can account for the complex neighborhood-scale effects of segregation in order to forecast neighborhood scale dynamics such as neighborhood migration.

Although there is a rich history of methods aimed at quantifying neighborhood-scale segregation and understanding its causes, it has been difficult to use these methods to accurately create forecasts of future changes in neighborhood-level population distributions. One general approach to the analysis of human segregation relies on the use of numerical indices to characterize the degree of segregation of a neighborhood [28, 29, 30, 31, 32, 33, 34, 35, 36, 37, 38]. Such

indices have been essential to understanding how segregation correlates with residential outcomes as well as potential drivers of segregation. Recently, Ellis et al [38] even used such indices to extrapolate which neighborhoods are more likely to change their degree of segregation, but stopped short of forecasting population changes, presumably because such indices are too coarse grained to make accurate predictions. Another approach utilizes agent-based models [39, 40, 41, 42, 43, 44, 45, 46, 47, 48, 49], such as the well studied Schelling model [39, 40, 41, 42, 43, 46], to determine the degree to which different proposed interactions lead to segregation. Such studies have shown that even slight preferences towards segregated neighborhood compositions can lead to drastic city-wide segregation. Since these models require *a priori* knowledge of the decision rules for migration that are challenging to determine, however, they have not been practical for predicting trends in human populations. Thus, despite great progress in understanding the nature of segregation, neither segregation indices nor agent-based models have led to accurate methods for predicting population dynamics at the neighborhood scale.

Recently, a new statistical physics method called Density-Functional Fluctuation Theory (DFFT) was developed to make predictions of how crowds will distribute in different environments [50]. DFFT is a top-down data-driven approach that extracts functions to separately quantify effective social and spatial preferences from observations of fluctuations in the local density. By recombining these functions, DFFT is able to forecast population distributions in new environments and with different total population numbers.

Here, we demonstrate how to extend DFFT to predict neighborhood-scale demographic data for multi-component time-dependent systems. We test this approach on data generated from an extended Schelling model simulation of residential segregation. We first describe application of the Schelling model to systems comprised of two types of agents in heterogeneous environments. We use the results generated from these simulations to create the demographic steady-state data for our analysis (Fig. 1a, Section 2). Second, we apply DFFT to this data and extract functions describing the effective spatial and social preferences of the population (Fig. 1b, Section 3). Importantly, this quantification of preferences is generic so that it can capture cumulative effects of the drivers of segregation without making specific assumptions about their properties or relative strengths. Next, we institute a sudden regional-scale demographic change to achieve a redistribution of the populations. We again use the Schelling model to generate the time evolution and new steady-state distribution of the neighborhood-scale demographic data. To predict the time evolution of the demographic data, we develop a time-dependent version of DFFT (TD-DFFT) using the extracted DFFT functions. We then compare the predictions from TD-DFFT to the data generated by the Schelling model (Fig. 1c, Section 4). Finally, we predict the new steady-state joint densities resulting from the demographic change, either through numerical computation using TD-DFFT or analytic calculation using the DFFT functions extracted from the original steady-state data. These predictions are then compared to the Schelling model data for the new steady state (Fig. 1d, Section 5). While we demonstrate this approach on data generated from a Schelling model, it should be possible to apply this method to publicly available demographic population counts for real populations. If application to real data is successful, DFFT would extend predictions at the regional-scale down to the neighborhood scale and yield valuable new insights and predictive power to the fields of segregation and migration.

2 Modified Schelling Simulation

To generate sample demographic data, we use a dynamic Schelling-type agent-based model [43] modified to include spatial dependence. In this model, two type of agents, 1000 red and 1000 blue, make probabilistic moves to new empty cells on a 60-by-60 lattice grid with periodic boundary conditions (Fig. 2a). The moves are based on changes in utility functions that specify social (“Social Utility” U_R^{so}, U_B^{so}) and spatial (“Spatial Utility” U_R^{sp}, U_B^{sp}) preferences. In particular, at each step in time, we randomly choose an agent and an empty cell, and the agent will move to the empty cell with probability

$$P = \begin{cases} \frac{1}{1 + e^{-\Delta(U_R^{so} + U_R^{sp})}} & \text{if agent is red} \\ \frac{1}{1 + e^{-\Delta(U_B^{so} + U_B^{sp})}} & \text{if agent is blue} \end{cases}, \quad (1)$$

where Δ denotes the change in utilities due to the proposed move [51] so that agents are more likely to move if the total utility increases. The social and spacial utility functions are defined in figures 2b,c and 2d,e respectively. In this particular case, we define the social utility of an agent to linearly increase with the number of 8-connected neighbors (dashed box in Fig. 2a) that are of the same type. This dependence is illustrated by the homogeneous color of the columns and rows in figures 2b and 2c respectively. We set the spatial utilities as shown in figure 2d,e, where red agents prefer the West side of the city and blue agents prefer the South side of the city. Additional results for more complex social utility functions are presented in the SI. We use these simulations to generate the data throughout this

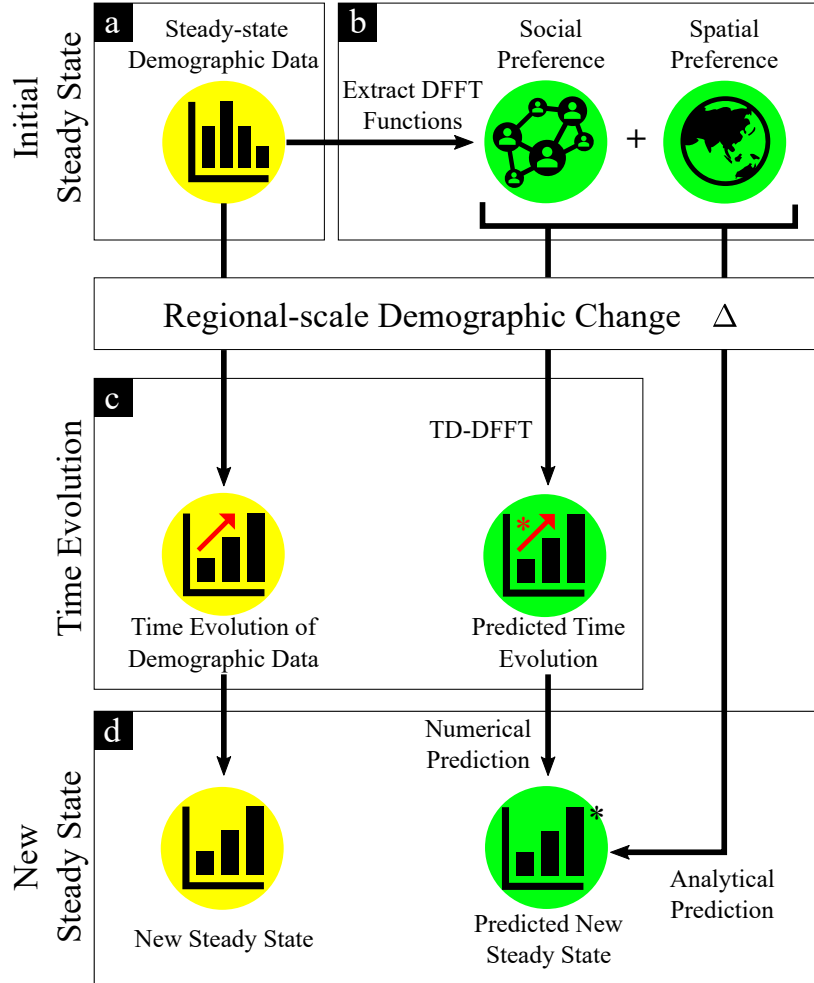


Figure 1: **General Workflow of Applying DFFT to Demographic Data** (a.) Collect neighborhood-scale steady-state demographic data in the form of probability distributions of local densities. In our example, we simulate the steady-state data from a Schelling model. (b.) Extract DFFT functions from steady-state data. The DFFT functions characterize social and spatial preferences separately. (c.) After a demographic change, we predict the time evolution of neighborhood-scale demographic data with TD-DFFT using the extracted DFFT functions. We compare our prediction with the observed time evolution from the Schelling model simulations. (d.) We predict the new neighborhood-scale steady state after the regional-scale demographic change either numerically using TD-DFFT or analytically using DFFT functions alone. We compare our prediction with the observed new steady state of the Schelling model simulations.

paper.

From these simulations we obtain coarse grained data of local agent densities and their steady-state joint probability distributions. In particular, we run an ensemble of Schelling simulations, wait until they reach a steady state, where the system fluctuates about a constant average distribution, and determine the agent configuration for each simulation. A sample steady-state configuration is shown in figure 2f. We coarse-grain the Schelling lattice grid into 25 blocks (outlined in the figure by thick lines) and record the total number of red agents $N_{R,b}$ and blue agents $N_{B,b}$ in each block b . Since all the blocks have the same area, $N_{R,b}$ and $N_{B,b}$ indicate local densities. By sampling the different steady-state configurations (denoted in the figure by the stack and ellipses) we measure the joint local probability distribution of agent densities for each block $P_b(N_{R,b}, N_{B,b})$. For simplicity, we will abbreviate $N_{R,b}$ and $N_{B,b}$ as N_R and N_B when there is no ambiguity. We show the joint probability distributions for the North East (NE), South West (SW) and South East (SE) blocks in figure 2g. We find that the SE block is likely to be occupied by a high density of blue agents, while the NE block is likely to be occupied by a low density of red and blue agents. We also find that the SW block is occupied by high densities of agents with a wide distribution of red and blue agent compositions. This wide distribution reflects the inherent biases for red and blue agents to segregate.

3 2-Component Density-Functional Fluctuation Theory

Single-component Density-Functional Fluctuation Theory conjectures that, by observing the steady-state probability distribution of a single type of agent in a block, one can extract information about the location dependent preferences and social interactions of the agent [50]. In particular, by observing the means of the distributions, it is possible to rank the agent preference for each block. Further, the shapes of the distributions provide information about social preference. For example, a Poisson-like distribution indicates no social interactions, a narrowly peaked distribution indicates strong repulsion, and a bimodal distribution indicates strong attractive interactions. As such, Mendez et al. [50] write the block dependent probability distribution as:

$$P_b(N) = z_b^{-1} \frac{1}{N!} \exp[-v_b N - f(N)], \quad (2)$$

where z_b^{-1} is a normalization constant; v_b is defined as the ‘‘vexation’’ and is constant for each block b ; and $f(N)$ is defined as the ‘‘frustration’’ and is block-independent function of local densities. Since all the blocks have the same area (See SI for the general case), the number of agents N indicates the density. When $f(N)$ is zero, the distribution is Poisson and the mean is proportional to $\exp[-v_b]$, indicating agents avoid blocks with high v_b . The deviation of the distribution from Poisson is captured by the function $f(N)$ that depends only on the density of agents. When $f(N)$ is concave up (e.g. P_b is narrowly peaked), agents disperse or segregate. When $f(N)$ is concave down (e.g. P_b is bimodal), agents aggregate. Thus, frustration and vexations respectively capture effective social and spatial interactions at the coarse-grained block scale. In previous work, it was shown that this functional form for the probability distribution is remarkably accurate for data on crowd distributions in not only model, but also living systems [50].

Extending this theory to multiple agents requires that we use a multivariate Poisson distribution to describe the block dependent vexations for all types of agent. Additionally, the frustration capturing the interactions between all the agents becomes a joint function of the density of each type of agent. For the case of two types of agents (Red and Blue) discussed in the present work, the steady-state joint probability distribution in each block b is given by:

$$P_b(N_R, N_B) = z_b^{-1} \frac{1}{N_R! N_B! (s - N_R - N_B)!} \exp[-v_{R,b} N_R - v_{B,b} N_B - f(N_R, N_B)], \quad (3)$$

where z_b^{-1} is, again, a normalization constant; $v_{R,b}$ and $v_{B,b}$ are the block-dependent vexations for the Red and Blue agents; and $f(N_R, N_B)$ is the block-independent frustration and is a function of the local densities of Red and Blue agents. As before, agents avoid blocks with high vexation. The frustration now captures the social interaction between two types of agents. Therefore, instead of a single curve that depends on the number of agents, the frustration becomes a surface that depends on the density of blue and the density of red agents. The concavities of curves on this surface indicates the social preferences for having greater or fewer agents of a particular type. Thus, this frustration function is a functional measure of segregation and can capture a variety of segregation behaviors (SI Section S6). Finally, the term $1/(s - N_R - N_B)!$ is introduced to better account for the fact that each block in our system can fit a maximum density of $s = 144$ agents (See SI Section S1 for a detailed derivation of equation (3)).

To determine whether this functional form for the probability distribution can be used to fit the Schelling model data we rearrange equation (3) to obtain

$$-\ln[N_R! N_B! (s - N_R - N_B)! P_b(N_R, N_B)] = f(N_R, N_B) + v_{R,b} N_R + v_{B,b} N_B + c_b, \quad (4)$$

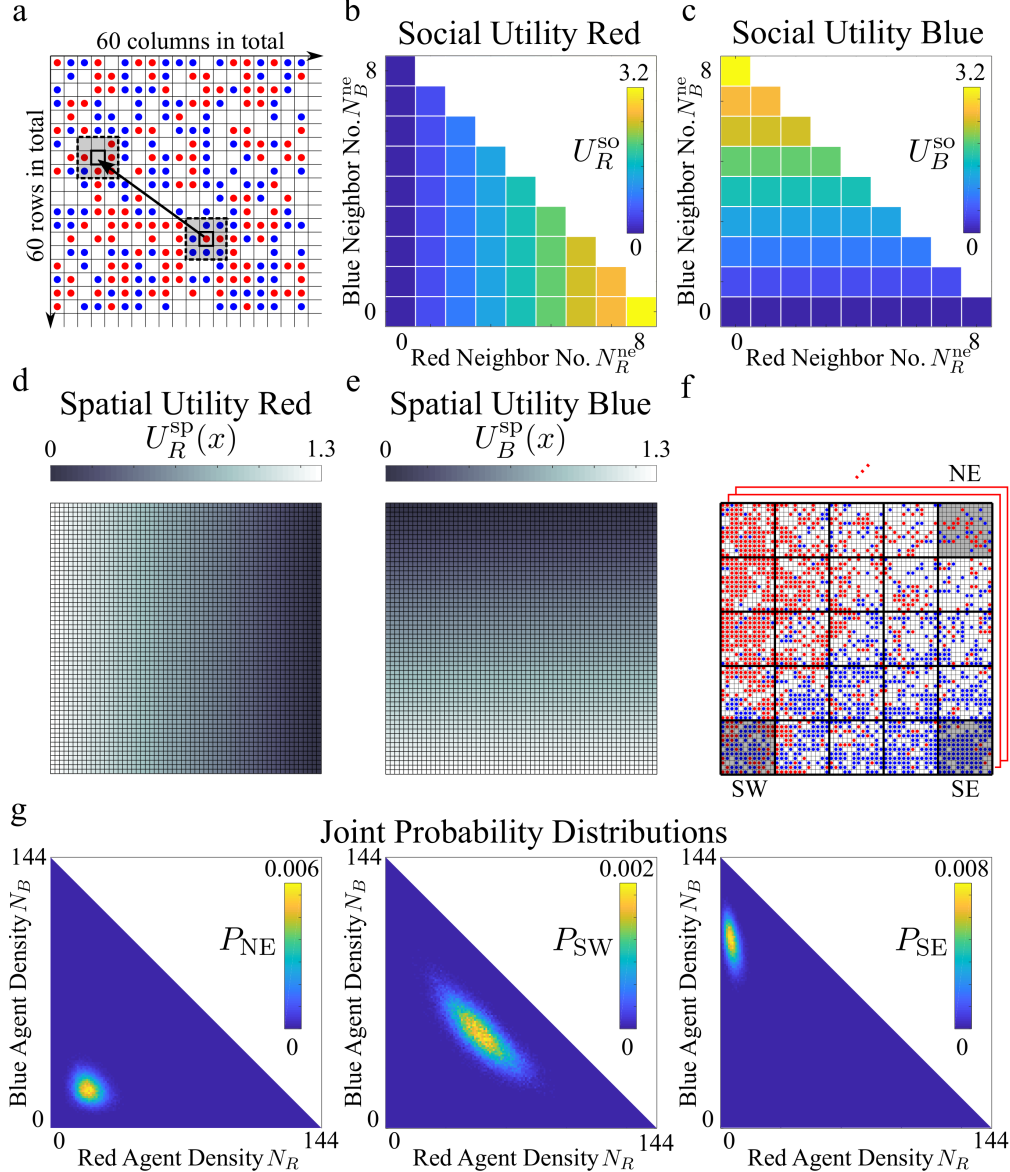


Figure 2: **Extended Schelling-type simulation and steady-state data (a.)** The Top-left corner of the Schelling lattice grid with 1000 red and 1000 blue agents. At each step in time, an agent and an empty cell are randomly chosen, and the agent will make probabilistic move to the empty cell. In this case, the red agent is chosen with arrow showing its proposed move to a randomly chosen empty cell. The 8-connected neighborhood (consisting of the 8 surrounding cells) of the red agent for its current or proposed cell are shown as dashed boxes. Due to the periodic boundary condition, the neighborhood of the empty cell looks disconnected. **(b.)** Social Utility for red agents is defined by $U_R^{so}(N_R^{ne}, N_B^{ne}) = 0.4 \cdot N_R^{ne}$, where N_R^{ne} and N_B^{ne} are the number of 8-connected red and blue neighbors respectively. For the red agent in **a**, the change in social utility due to the proposed move is given by $U_R^{so}(5, 1) - U_R^{so}(1, 6) = +1.6$, making this move more socially attractive. **(c.)** Social Utility for blue agents is defined by $U_B^{so}(N_R^{ne}, N_B^{ne}) = 0.4 \cdot N_B^{ne}$. **(d.)** Spatial Utility for red agents $U_R^{sp}(x)$ is a function of location x , that decreases linearly in the horizontal direction. The change in spatial utility for the red agent in **a** for the proposed move is $\Delta U_R^{sp} \approx +0.17$, making this move more spatially attractive. So, according to Equation (1), the red agent has a 85% chance of moving. **(e.)** Spatial Utility for blue agents $U_B^{sp}(x)$ is a function of location x , that decreases linearly in the vertical direction. **(f.)** A sample steady-state configuration of our simulation after reaching steady state (> 10000 steps). We divide the Schelling lattice grid into 25 blocks, three of which are shaded and labeled as 'NE', 'SW', and 'SE' for reference. To obtain a collection of steady-state configurations (red stack and red ellipses), we run an ensemble of Schelling simulations. **(g.)** From the collection of steady-state configurations, one can observe the steady-state joint probability distribution of agent densities for each block. Distributions for blocks 'NE', 'SW', 'SE' are shown.

where $c_b = \ln(z_b)$ is a normalization constant. The LHS of Equation (4) is determined by our observed probability P_b , and is plotted for three sample blocks in figure 3a.

We use a Maximum Likelihood Estimation algorithm to infer the frustration and vexations that best fit the data and plot these in figure 3b. We find that the fits are remarkably accurate as illustrated by the small errors (differences between LHS and RHS of equation (4)) shown for three sample blocks in figure 3c. The extracted frustration and vexations can then be used to predict how populations will redistribute in response to demographic changes, as we show next.

4 Predicting Time Evolution

To generate a demographic change in the simulation data, we abruptly switch 350 randomly chosen red agents on the north side of the Schelling lattice into blue agents. We then record the evolution of an ensemble of agent configurations (illustrated by the stack and ellipses) as it transitions from this new altered state at $t = 0$ to the new steady state at $t \rightarrow \infty$ (Fig. 4a). As before, we coarse grain these data at the block level to extract the density of red and blue agents at each time. The challenge is to predict the evolution of these neighborhood-scale data using DFFT parameters extracted from the initial steady state data and knowledge of the regional-scale demographic change. Note that an abrupt regional-scale demographic change should result in a more extreme neighborhood-scale time evolution, and therefore be harder to predict than a more realistic continuous demographic change over time.

4.1 Time-Dependent DFFT model (Kohn-Sham TD-DFFT)

To predict the evolving joint density distributions of the ensemble described above, we construct a Time-Dependent DFFT model in which agents choose to move from block to block based on changes in the coarse-grained spatial and social preferences. The coarse-grained preferences can be combined into block-level ‘‘Headache’’ functions:

$$H_b(N_R, N_B) = v_{R,b}N_R + v_{B,b}N_B + f(N_R, N_B). \quad (5)$$

Specifically, at every step in time, we choose an agent randomly and choose a block with a weight proportional to the amount of empty spaces it has. The agent then moves from its current block b to the chosen block b' with probability:

$$P_{b \rightarrow b'} = \frac{1}{1 + e^{\Delta H_b + \Delta H_{b'}}}, \quad (6)$$

where Δ denotes the change due to the proposed move. By evolving the ensemble of altered states according to the above rule, we can numerically predict the evolution of the joint density distributions, up to a constant-time scale difference (See SI Section S8 for reasons of introducing a time scale). We can extract the time scale easily by comparing the rate of steady-state fluctuations in the Schelling simulation and the TD-DFFT model. This TD-DFFT model corresponds to the adiabatic approximation of Kohn-Sham Time-Dependent Density-functional Theory [52, 53, 54] (See SI Section S9), whose predictions can be determined exactly through a master equation approach as well (See SI Section S8).

4.2 Mean Value Equation (Hohenberg-Kohn TD-DFFT)

For situations where the full analysis presented above is too computationally expensive, we develop a simplified mean value approach. In particular, to obtain a good distribution of states, the above agent-based simulation approach to solving Kohn-Sham TD-DFFT model requires that we evolve an ensemble with a size much bigger than the number of frequently observed states. Since the number of states scales steeply with the number of blocks and agents, the Kohn-Sham TD-DFFT model may be computationally expensive to run for real cities with hundreds of blocks and millions of people. When the probability distributions are single-peaked, as is the case here, one may approximate the time evolution of the joint mean densities of the above model according to the following Mean Value Equation (MVE, See derivation in SI Section S8):

$$\begin{cases} \frac{d}{dt} \overline{N_{R,b}} = \sum_{b' \neq b} \nu_{R,b' \rightarrow b} - \nu_{R,b \rightarrow b'} \\ \frac{d}{dt} \overline{N_{B,b}} = \sum_{b' \neq b} \nu_{B,b' \rightarrow b} - \nu_{B,b \rightarrow b'} \end{cases}, \quad (7)$$

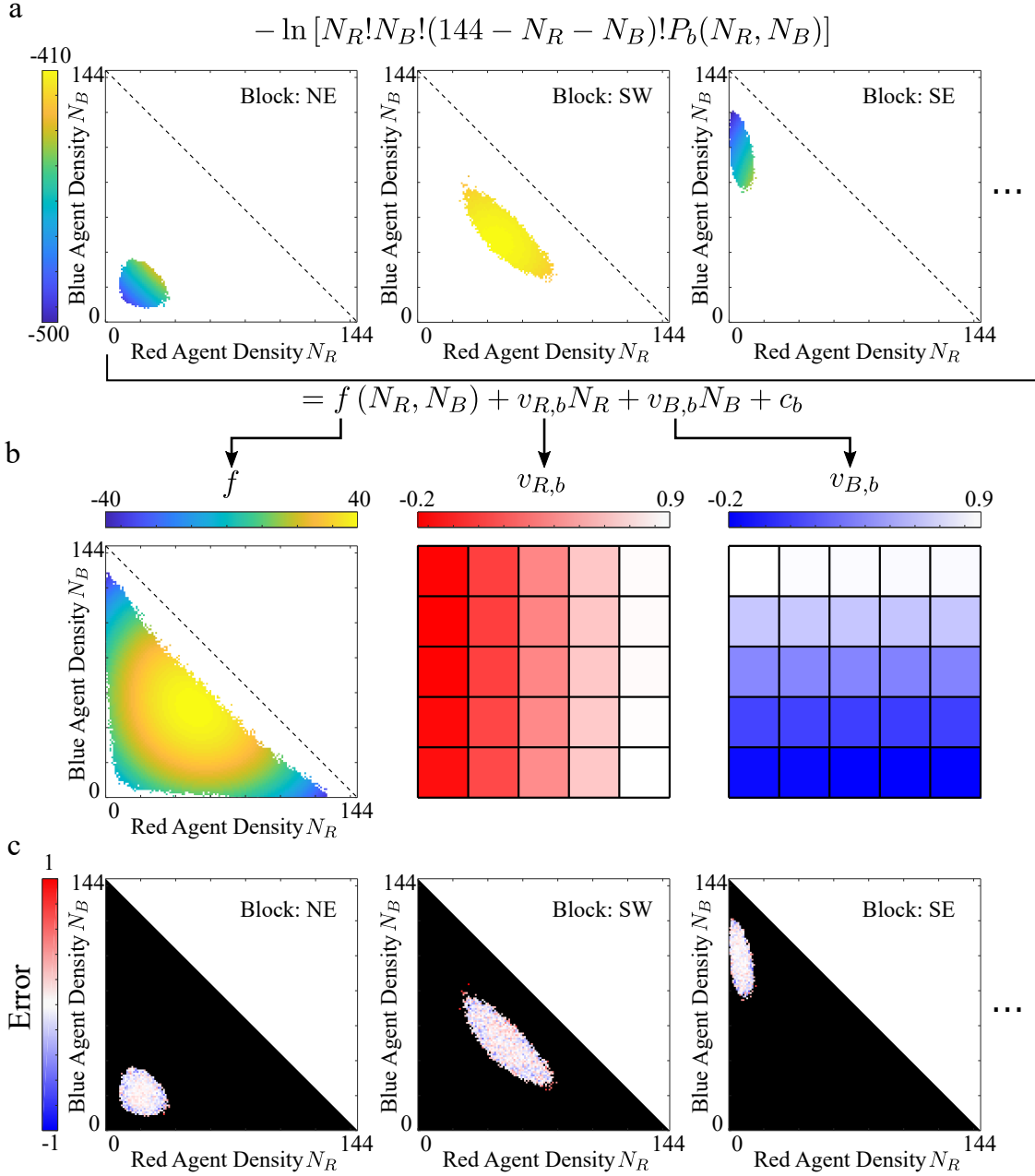


Figure 3: **Extracting effective social and spatial preferences (a.)** The LHS of Equation (4) is determined by our observed probability P_b (Fig. 2g), and is plotted for blocks 'NE', 'SW', 'SE'. We only keep data for cases where more than 10 observations are recorded for a particular agent combination. **(b.)** Using Maximum Likelihood Estimation, we fit each of the 25 LHS surfaces by a block-independent surface called "frustration" together with a block-dependent planar shift $v_{R,b}N_R + v_{B,b}N_B + c_b$, where $v_{R,b}$ and $v_{B,b}$ are two block-dependent constants called "vexations", and c_b is a block-dependent normalization constant. Frustration describes social preference, while vexations describe spatial preference. **(c.)** The errors of the fit in **b** are determined by the difference between the right hand and left hand sides of equation (4), for the NE, SW, and SE blocks.

where $\overline{N_{R,b}}$ and $\overline{N_{B,b}}$ denotes the mean red and blue agent density for block b , respectively. $\nu_{R,b \rightarrow b'}$ and $\nu_{B,b \rightarrow b'}$ are the density flow rates for red and blue agents from block b to block b' , calculated from

$$\begin{cases} \nu_{R,b \rightarrow b'} \approx \frac{\overline{N_{R,b}}}{N_{\text{tot}}} \cdot \frac{s - \overline{N_{R,b'}} - \overline{N_{B,b'}}}{s_{\text{tot}} - N_{\text{tot}}} \cdot P_{b \rightarrow b'} \\ \nu_{B,b \rightarrow b'} \approx \frac{\overline{N_{B,b}}}{N_{\text{tot}}} \cdot \frac{s - \overline{N_{R,b'}} - \overline{N_{B,b'}}}{s_{\text{tot}} - N_{\text{tot}}} \cdot P_{b \rightarrow b'} \end{cases} \quad (8)$$

Equation (7) says that the rate of change in the mean density of agents in block b is given by the sum of inflow rates from all other blocks $b' \neq b$ into block b , minus the sum of outflow rates from block b into all other blocks $b' \neq b$. We can also easily interpret the flow rate approximations in Equation (8) following the rules of the TD-DFFT Model (Section 4.1): The first term in the product represents the probability of choosing the corresponding type of agent in block b , where the denominator $N_{\text{tot}} = 2000$ is the total number of agents in the city; The second term in the product represents the probability of choosing an empty cell in block b' , where the denominator $s_{\text{tot}} - N_{\text{tot}} = 3600 - 2000 = 1600$ is the total number of empty cells in the city; The third term corresponds to the probability of transition defined in Equation (6). Note that this MVE might fail to capture the behavior of the TD-DFFT Model with extreme segregation, when Equation (7) exhibits ‘bifurcation behavior’ [22, 25] (See SI Section S10). Since the MVE deals with average numbers in each block, it corresponds more closely to a Hohenberg-Kohn [55] TD-DFT (See SI Section S9).

4.3 Results

Overall, we obtain excellent agreement between the TD-DFFT model/MVE predictions and the simulated Schelling data. As an example, we compare the predicted (Figs. 4b,c) and observed (Figs. 4d,e) time evolution of the probability distribution of red (N_R) and blue (N_B) agents for the South East (SE) block (and all other blocks in SI Section S12). We find that the model accurately captures the trends in the means as well as the skews in the distributions about the means. In particular, the MVE (blue dotted lines in Figs. 4b,c) accurately tracks the mean values of the TD-DFFT model (red lines in Figs. 4b,c). Additionally, we compare the trajectory of the joint means for all the blocks in figure 4f. Once again, we find excellent agreement throughout the entire trajectory even when the evolution is non-monotonic as is the case for blocks 12-15. Finally, given an initial joint density (N_R, N_B) for a particular block we are able to predict the joint probability distribution for the block after 1000 Schelling steps. We plot the observed average change in the joint density for each initial condition for the SE block in figure 4g. These predictions, indicated by the red arrows, are compared with the observed data, indicated by the black arrows. Once again, we observe excellent agreement between the predictions of the TD-DFFT model and the demographic data. The arrow directions reflect the constraints induced by local interactions over short time scales, despite the fact that the long time equilibrium of the joint probability distribution resides in the upper left region of the plot. It is this capacity to model the step-wise evolution that allows the TD-DFFT model to accurately track the time dependent trajectories of the Joint Means as shown in figure 4f. Finally, we have conducted similar studies involving the same demographic change for cases where the demographic data is generated using more complicated Social and Spatial utility functions and have obtained TD-DFFT predictions of similar fidelity.

In part, the reason the Time-dependent DFFT model is able to accurately describe the evolution of the Schelling data after a demographic change, is that it is itself a type of agent-based model. There are, however, a number of important distinctions. First, the TD-DFFT model relies on coarse-grained data. Details of the Schelling simulation such as the lattice grid structure, the 8-connected neighbors, and empty spots are averaged over to obtain the density in each block. As such the TD-DFFT model keeps only the essential information necessary to make predictions about the density. Second, the TD-DFFT model relies on empirically extracted parameters. As such it does not require that we impose specific rules governing the system evolution. Instead, it determines the rules from the original steady-state data in order to make predictions. These distinctions will lead to discrepancies in certain extreme conditions. For instance, when block-size is very small (e.g. 4 by 4 cells), the interaction of agents between neighboring blocks will greatly affect the dynamics. In the TD-DFFT model, however, such effects are ignored in the coarse-graining procedure, resulting in different dynamics (See SI, Section S13).

5 Predicting the New Steady-state

To predict the new steady-state joint probability distributions, $P_b(N_R, N_B, t \rightarrow \infty)$ we can either run the TD-DFFT model until it reaches a steady state, or calculate the new distribution analytically. To analytically predict the new distribution, we take advantage of the fact that the social and spatial preferences of the individuals remain the same throughout this demographic change in the total number of each agent. Since these social and spatial preferences manifest themselves at the coarse grained level as differences in the headache functions of two blocks, $\Delta H_b + \Delta H'_b$,

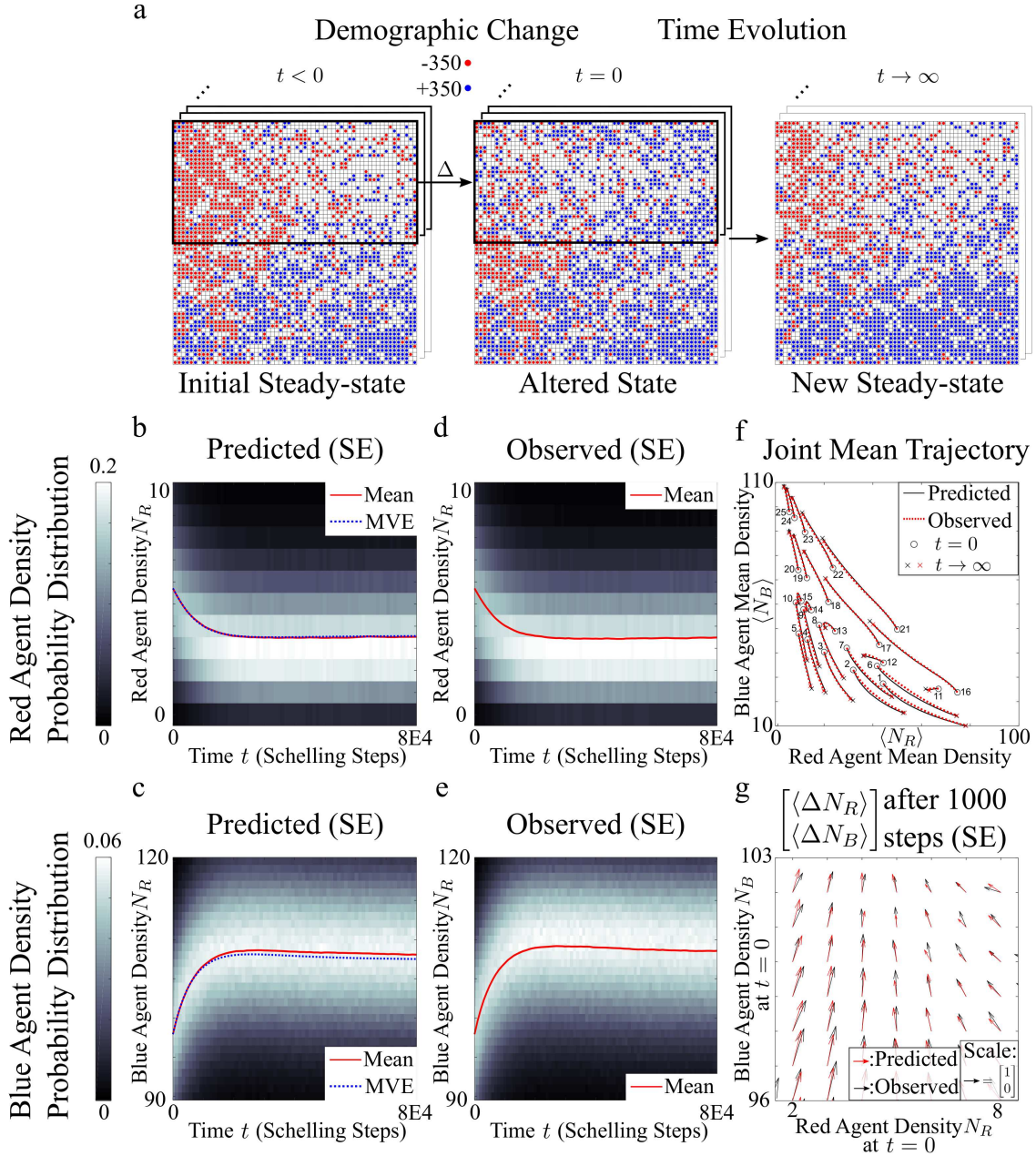


Figure 4: **Predicting time evolution** (a.) Starting from a steady-state configuration, at $t = 0$, we introduce our demographic change by abruptly switching 350 randomly chosen red agents on the north side of the Schelling lattice into blue agents to obtain an altered state. The system is then evolved according to the Schelling model. The above procedure is repeated over an ensemble of Schelling simulations (shown as stacks and ellipses). (b.,c.) Predicted time evolution of the probability distribution for observing red or blue agents for the 'SE' block using the TD-DFFT model. Note that the distribution for red agent is skewed away from the mean towards more segregated values. The MVE predictions agree well with the TD-DFFT Model. (d.,e.) Observed time evolution of the probability distribution for observing red or blue agents for the 'SE' block from the Schelling simulation. (f.) Observed versus predicted Joint-mean density trajectories for all blocks (counted left-to-right then top-to-bottom, in normal English reading order). Blocks 13-15 show interesting trajectories, which TD-DFFT model predict well. (g.) Observed versus predicted average changes in number of agents in block 'SE' after 1000 Schelling steps for various initial number of agents. We note that a calibration factor is necessary to match the time scales between the density based model predictions and the Schelling simulation time steps.

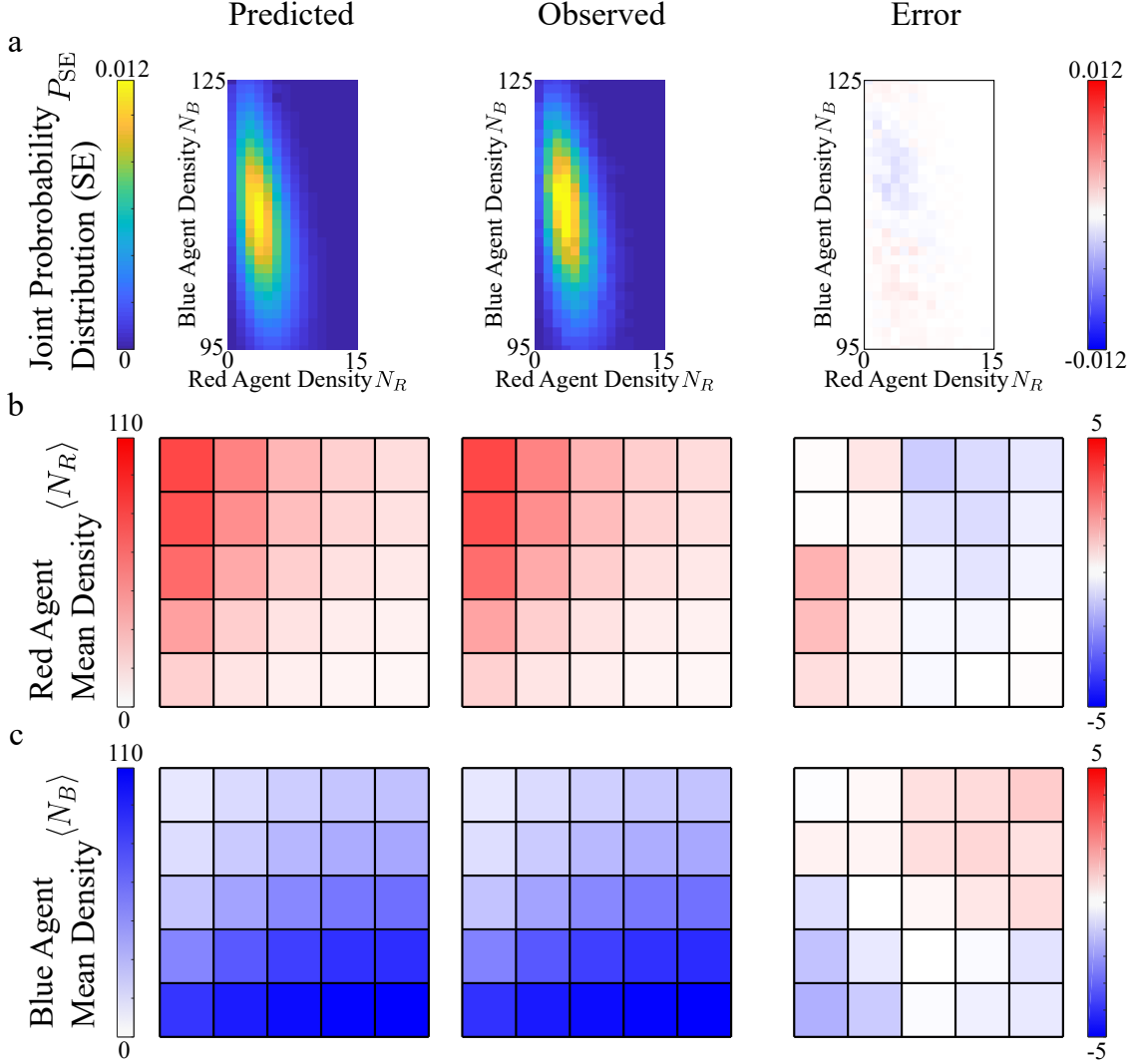


Figure 5: **Analytically predict new steady state (a.)** Predicted versus observed new steady-state joint probability distribution for block 'SE'. **(b.)** Predicted versus observed mean densities of red agents for all blocks. **(c.)** Predicted versus observed mean densities of blue agents for all blocks.

we can rewrite the headache function as:

$$H_b \longrightarrow H_b - \mu_R N_R - \mu_B N_B \quad (9)$$

without affecting these preferences. Here, μ_R and μ_B are block-independent constants called 'agent potentials' (analogous to chemical potentials in statistical physics) that tune the expected total number of each type of agent over all the blocks (see SI, Sections S1 and S11). To determine these constants, we modify the exponent in Eq. 3 and use Newton's method to converge on values for μ_R and μ_B so that the means of the probability distribution, when averaged over all the blocks, equals the new mean for the entire system resulting from the demographic change. We compare the predictions for the joint probability distributions, as well as the mean of the agent densities for each block with the observed data from the Schelling model in figure 5 and SI Section S12. We find excellent agreement between the predictions and the simulated demographic data. Importantly, this analytic approach arrives at the same new steady state distribution that the previously described time dependent DFFT model predicts, but with orders of magnitude increase in computational speed and without the need for modelling dynamic behaviors.

6 Implications and Future Directions

The ability of DFFT to accurately predict the evolution of residential segregation for demographic data obtained from the Schelling model is an important step towards developing methods for making demographic predictions. Unlike bottom-up agent-based approaches that postulate specific rules, DFFT empirically extracts these rules from observations. Additionally, in contrast to top-down data-driven approaches that only extract descriptive measures of segregation, DFFT uses the more detailed extracted rules to forecast population dynamics.

Importantly, this framework could easily be extended to include an even greater number of agent types. As long as residential choice is driven separately by the composition of local neighborhoods and the coarse agent spatial preferences, it is straightforward to include vexations for each agent type and a multidimensional frustration that accounts for the multi-agent social interactions.

We also anticipate a clear pathway towards modeling other demographic changes such as changes in social or spatial preferences. In these particular cases it is necessary to know how to map such changes to the DFFT functions extracted from the initial steady state data. Such a mapping can be achieved in a number of ways. First, it may be possible to directly guess the change in the DFFT functions. For example, if we knew that the spatial utility functions for the agents were exchanged, we could use knowledge from previous simulations to determine the new vexations: $v_B \rightarrow v_R$ and $v_R \rightarrow v_B$. Second, even if we had no *a priori* knowledge of this change, we could still use intermediate time points in the evolution of the demographic data to adjust the vexations and frustration. For example, after every 500 Schelling time steps we would modify our DFFT functions so that we get the best agreement between the dynamics of the predicted and observed density changes for the agents (Fig. 4g). These examples illustrate the flexibility that DFFT provides for making predictions for a broad range of demographic changes within the context of the Schelling model.

The ability to recast the Schelling model into the DFFT framework suggests that it should be possible to extend this approach to other agent based models. In the field of ecological demography, DFFT could provide a new description for predator-prey dynamics in the stochastic spatial Lotka-Volterra model [56]. In the fields of evolutionary biology or economics, DFFT could give new insights into the success of different strategies such as cooperation by coarse graining stochastic game models [57, 58]. As long as the agents in a given system are driven separately by local interactions with their neighbors and spatial interactions, we expect the DFFT analysis presented here will make accurate predictions of the evolving system.

Finally, to the extent that agent-based approaches like the Schelling model inform trends in human demographic data, it may be possible to apply DFFT to data sets for human populations. For example, decennial American census data provides block level counts of the number of people by race and ethnicity. Given these data, DFFT could be used to measure the frustration between different races or ethnicities and their vexations throughout the country. As such DFFT could serve as a detailed lens into the social and spatial nature of racial residential segregation and be a powerful tool for forecasting the composition of block level demographics.

7 Authors' Contributions

T.A.A. developed initial theoretical extensions to DFFT work including multi-component and time-dependent systems. Y.A.K. and I.C. proposed initial application of DFFT onto demographic systems. M.H. provided context of proposed methods within the broader field of demography. Y.C., Y.A.K., B.B., T.A.A. and I.C. developed and refined multi-component and time-dependent applications of DFFT onto simulated data. Y.C. implemented all simulations, performed all analyses of data, and created all figures. Y.A.K. wrote code for statistical extraction of parameters from data. Y.C. wrote initial draft of paper and SI. I.C. and Y.A.K. performed extensive edits to paper. I.C. mentored Y.C. and Y.A.K.. T.A.A. mentored Y.C. and B.B..

8 Acknowledgements

The authors thank The Cohen and Arias groups for helpful discussions throughout this work. The work was funded by NSF BRAIN EAGER 1546710, ARO W911NF-18-1-0032, and NIH R01NS116595-01 grants. Y.K. was also supported in part by funding from the National Science Foundation Graduate Research Fellowship Award No. DGE-1650441. B.B. was supported in part by funding from the Postgraduate Scholarship-Doctoral (PGS D) from the Natural Sciences and Engineering Research Council of Canada (NSERC).

References

- [1] Jacob S. Siegel and David A. Swanson. *The Methods and Materials of Demography*. Emerald Group Publishing Limited, 2004.
- [2] David A Swanson et al. “K-12 enrollment forecasting: merging methods and judgment.” In: *ERS spectrum* 16.4 (1998), pp. 24–31.
- [3] John S Humphreys. “Delimiting ‘rural’: implications of an agreed ‘rurality’ index for healthcare planning and resource allocation”. In: *Australian Journal of Rural Health* 6.4 (1998), pp. 212–216.
- [4] Jeff Tayman, Bob Parrott, and Sue Carnevale. “Locating fire station sites: The response time component”. In: *RAND-PUBLICATIONS-MR-ALL SERIES-* (1997), pp. 203–217.
- [5] Andrew Mason. “Population and housing”. In: *Population Research and Policy Review* 15.5-6 (1996), pp. 419–435.
- [6] Laurie M Anderson et al. “Providing affordable family housing and reducing residential segregation by income: a systematic review”. In: *American journal of preventive medicine* 24.3 (2003), pp. 47–67.
- [7] Metropolitan Washington Council of Governments. *Here’s how we use growth forecasts for transportation planning*. 2018. URL: <https://www.mwcog.org/newsroom/2018/03/05/heres-how-we-use-growth-forecasts-for-transportation-planning/>. (accessed: 07.23.2020).
- [8] Gerard C Wellman. “Transportation apartheid: the role of transportation policy in societal inequality”. In: *Public Works Management & Policy* 19.4 (2014), pp. 334–339.
- [9] Donald T Rowland. “Demographic methods and concepts”. In: *OUP Catalogue* (2003).
- [10] Samuel Preston, Patrick Heuveline, and Michel Guillot. *Demography: Measuring and Modeling Population Processes*. Wiley-Blackwell, 2000.
- [11] Stanley K Smith, Jeff Tayman, and David A Swanson. *A practitioner’s guide to state and local population projections*. Springer, 2013.
- [12] Kenneth W Wachter. *Essential demographic methods*. Harvard University Press, 2014.
- [13] Nathan Keyfitz and Hal Caswell. *Applied mathematical demography*. Vol. 47. Springer, 2005.
- [14] Kenneth C Land, Yang Yang, and Yi Zeng. “Mathematical demography”. In: *Handbook of population*. Springer, 2005. Chap. 22, pp. 659–717.
- [15] Andrei Rogers. “Demographic modeling of the geography of migration and population: A multiregional perspective”. In: *Geographical Analysis* 40.3 (2008), pp. 276–296.
- [16] Raul Ramos and Jordi Suriñach. “A Gravity Model of Migration Between the ENC and the EU”. In: *Tijdschrift voor economische en sociale geografie* 108.1 (2017), pp. 21–35.
- [17] Jeffrey Grogger and Gordon H Hanson. “Income maximization and the selection and sorting of international migrants”. In: *Journal of Development Economics* 95.1 (2011), pp. 42–57.
- [18] David Karemera, Victor Iwuagwu Oguledo, and Bobby Davis. “A gravity model analysis of international migration to North America”. In: *Applied Economics* 32.13 (2000), pp. 1745–1755.
- [19] Keuntae Kim and Joel E Cohen. “Determinants of international migration flows to and from industrialized countries: A panel data approach beyond gravity”. In: *International migration review* 44.4 (2010), pp. 899–932.
- [20] Jacques Poot et al. “The gravity model of migration: the successful comeback of an ageing superstar in regional science”. In: *IZA discussion paper* (2016).
- [21] David K Foot and William J Milne. “Net migration estimation in an extended, multiregional gravity model.” In: *Journal of regional science* 24.1 (1984), pp. 119–133.
- [22] Wolfgang Weidlich and Günter Haag. *Concepts and models of a quantitative sociology: the dynamics of interacting populations*. Vol. 14. Springer Science & Business Media, 2012.
- [23] Wolfgang Weidlich and Günter Haag. *Interregional migration: dynamic theory and comparative analysis*. Vol. 4. Springer, 1988.
- [24] Wolfgang Weidlich. *Sociodynamics: A systematic approach to mathematical modelling in the social sciences*. Courier Corporation, 2006.
- [25] Gunter Haag. *Modelling with the Master Equation: Solution Methods and Applications in Social and Natural Sciences*. Cham, Switzerland: Springer International Publishing, 2017.
- [26] William AV Clark. “Residential segregation in American cities: A review and interpretation”. In: *Population research and Policy review* 5.2 (1986), pp. 95–127.
- [27] Lance Freeman. “Neighbourhood diversity, metropolitan segregation and gentrification: What are the links in the US?” In: *Urban Studies* 46.10 (2009), pp. 2079–2101.

- [28] Sean F Reardon and Glenn Firebaugh. “Measures of multigroup segregation”. In: *Sociological methodology* 32.1 (2002), pp. 33–67.
- [29] Sean F Reardon and David O’Sullivan. “Measures of spatial segregation”. In: *Sociological methodology* 34.1 (2004), pp. 121–162.
- [30] Sean F Reardon. “A conceptual framework for measuring segregation and its association with population outcomes”. In: *Methods in social epidemiology* 1.169 (2006), pp. 169–192.
- [31] Yoo Min Park and Mei-Po Kwan. “Beyond residential segregation: A spatiotemporal approach to examining multi-contextual segregation”. In: *Comput. Environ. Urban Syst* 71 (2018), pp. 98–108.
- [32] Michael J White, Ann H Kim, and Jennifer E Glick. “Mapping social distance: Ethnic residential segregation in a multiethnic metro”. In: *Sociological Methods & Research* 34.2 (2005), pp. 173–203.
- [33] Masayoshi Oka and David WS Wong. “Capturing the two dimensions of residential segregation at the neighborhood level for health research”. In: *Frontiers in public health* 2 (2014), p. 118.
- [34] Masayoshi Oka and David WS Wong. “Spatializing Area-Based Measures of Neighborhood Characteristics for Multilevel Regression Analyses: An Areal Median Filtering Approach”. In: *Journal of Urban Health* 93.3 (2016), pp. 551–571.
- [35] Ricardo Mora and Javier Ruiz-Castillo. “Entropy-based segregation indices”. In: *Sociological Methodology* 41.1 (2011), pp. 159–194.
- [36] Christopher S. Fowler. “Segregation as a multiscale phenomenon and its implications for neighborhood-scale research: The case of South Seattle 1990–2010”. In: *Urban geography* 37.1 (2016), pp. 1–25.
- [37] Federico Echenique and Roland G Fryer Jr. “A measure of segregation based on social interactions”. In: *The Quarterly Journal of Economics* 122.2 (2007), pp. 441–485.
- [38] Mark Ellis et al. “Predicting neighborhood racial change in large US metropolitan areas, 1990–2010”. In: *Environment and Planning B: Urban Analytics and City Science* 45.6 (2018), pp. 1022–1037.
- [39] Thomas C Schelling. “Dynamic models of segregation”. In: *Journal of mathematical sociology* 1.2 (1971), pp. 143–186.
- [40] Junfu Zhang. “A dynamic model of residential segregation”. In: *Journal of Mathematical Sociology* 28.3 (2004), pp. 147–170.
- [41] Junfu Zhang. “Residential segregation in an all-integrationist world”. In: *Journal of Economic Behavior & Organization* 54.4 (2004), pp. 533–550.
- [42] Junfu Zhang. “Tipping and residential segregation: a unified Schelling model”. In: *Journal of Regional Science* 51.1 (2011), pp. 167–193.
- [43] Sebastian Grauwil, Florence Goffette-Nagot, and Pablo Jensen. “Dynamic models of residential segregation: An analytical solution”. In: *Journal of Public Economics* 96.1-2 (2012), pp. 124–141.
- [44] Dejan Vinković and Alan Kirman. “A physical analogue of the Schelling model”. In: *Proceedings of the National Academy of Sciences* 103.51 (2006), pp. 19261–19265.
- [45] William AV Clark and Mark Fossett. “Understanding the social context of the Schelling segregation model”. In: *Proceedings of the National Academy of Sciences* 105.11 (2008), pp. 4109–4114.
- [46] Elizabeth E Bruch and Robert D Mare. “Neighborhood choice and neighborhood change”. In: *American Journal of sociology* 112.3 (2006), pp. 667–709.
- [47] Arnout Van de Rijdt, David Siegel, and Michael Macy. “Neighborhood chance and neighborhood change: A comment on Bruch and Mare”. In: *American Journal of Sociology* 114.4 (2009), pp. 1166–1180.
- [48] Elizabeth E Bruch and Robert D Mare. “Preferences and pathways to segregation: Reply to van de Rijdt, Siegel, and Macy”. In: *American Journal of Sociology* 114.4 (2009), pp. 1181–1198.
- [49] Yu Zou et al. “Model reduction for agent-based social simulation: coarse-graining a civil violence model”. In: *Physical review E* 85.6 (2012), p. 066106.
- [50] J Felipe Méndez-Valderrama et al. “Density-functional fluctuation theory of crowds”. In: *Nature communications* 9.1 (2018), p. 3538.
- [51] Daniel McFadden et al. “Conditional logit analysis of qualitative choice behavior”. In: *Institute of Urban and Regional Development* (1973).
- [52] Walter Kohn and Lu Jeu Sham. “Self-consistent equations including exchange and correlation effects”. In: *Physical review* 140.4A (1965), A1133.
- [53] Erich Runge and Eberhard KU Gross. “Density-functional theory for time-dependent systems”. In: *Physical Review Letters* 52.12 (1984), p. 997.
- [54] M Thiele, EKU Gross, and S Kümmel. “Adiabatic approximation in nonperturbative time-dependent density-functional theory”. In: *Physical review letters* 100.15 (2008), p. 153004.

- [55] Pierre Hohenberg and Walter Kohn. “Inhomogeneous electron gas”. In: *Physical review* 136.3B (1964), B864.
- [56] Ulrich Dobramysl et al. “Stochastic population dynamics in spatially extended predator–prey systems”. In: *Journal of Physics A: Mathematical and Theoretical* 51.6 (2018), p. 063001.
- [57] Yu’e Wu, Shuhua Zhang, and Zhipeng Zhang. “Environment-based preference selection promotes cooperation in spatial prisoner’s dilemma game”. In: *Scientific reports* 8 (2018).
- [58] Martin A Nowak and Robert M May. “Evolutionary games and spatial chaos”. In: *Nature* 359.6398 (1992), p. 826.